

# Histogram of Gradient Orientations of Signal Plots applied to P300 Detection

Rodrigo Ramele, *Member, IEEE*, Ana Julia Villar, and Juan Miguel Santos

**Abstract**—The analysis of Electroencephalographic (EEG) signals is of ulterior importance to aid in the diagnosis of mental disease and to increase our understanding of the brain. Traditionally, clinical EEG has been analyzed in terms of temporal waveforms, looking at rhythms in spontaneous activity, subjectively identifying troughs and peaks in Event-Related Potentials (ERP), or by studying graphoelements in pathological sleep stages. Additionally, the discipline of Brain Computer Interfaces requires new methods to decode patterns from non-invasive EEG signals. This field is developing alternative communication pathways to transmit volitional information from the Central Nervous System. The technology could potentially enhance the quality of life of patients affected by neurodegenerative disorders and other mental illness. This work mimics what electroencephalographers have been doing clinically, visually inspecting and categorizing phenomena within the EEG by the extraction of features from images of signal plots. These features are constructed based on the calculation of histograms of oriented gradients from pixels around the signal plot. It aims to provide a new objective framework to analyze, characterize and classify EEG signal waveforms. The feasibility of the method is outlined by detecting the P300, an ERP elicited by the oddball paradigm of rare events, and implementing an offline P300-based BCI Speller. The validity of the proposal is shown by offline processing a public dataset of Amyotrophic Lateral Sclerosis (ALS) patients and an own dataset of healthy subjects.

**Index Terms**—electroencephalography, histogram of gradient orientations, brain-computer interfaces, P300, SIFT, amyotrophic lateral sclerosis, naive-bayes near neighbours, waveforms

## I. INTRODUCTION

ALTHOUGH recent advances in neuroimaging techniques, particularly radio-nuclear and radiological scanning methods [1], have diminished the prospects of the traditional Electroencephalography (EEG), the advent and development of digitized devices has impelled for a revamping of this hundred years old technology. Their versatility, ease of use, temporal resolution, ease of development and production, and its proliferation as consumer devices, are pushing EEG to become the de-facto non invasive portable or ambulatory method to access and harness brain information [2].

A key contribution to this expansion has been the field of Brain Computer Interfaces (BCI) [3] which is the pursuit of the development of a new channel of communication particularly aimed to persons affected by neurodegenerative diseases.

One noteworthy aspect of this novel communication channel is the ability to transmit information from the Central Nervous System (CNS) to a computer device and from there use that

information to control a wheelchair [4], as input to a speller application [5], in a Virtual Reality environment [6] or as aiding tool in a rehabilitation procedure [7]. The holy grail of BCI is to implement a new complete and alternative pathway to restore lost locomotion [3].

EEG signals are remarkably complex and have been characterized as a multichannel non-stationary stochastic process. Additionally, they have high variability between different subjects and even between different moments for the same subject, requiring adaptive and co-adaptive calibration and learning procedures [8]. Hence, this imposes an outstanding challenge that is necessary to overcome in order to extract information from raw EEG signals.

BCI has gained mainstream public awareness with worldwide challenge competitions like Cybathlon [9], [10] and even been broadcasted during the inauguration ceremony of the 2014 Soccer World Cup. New developments have overcome the out-of-the-lab high-bar and they are starting to be used in real world environments [11], [12]. However, they still lack the necessary robustness, and its performance is well behind any other method of human computer interaction, including any kind of detection of residual muscular movement [8].

A few works have explored the idea of exploiting the signal waveform to analyze the EEG signal. In [13] an approach based on Slope Horizontal Chain Code is presented, whereas in [14] a similar procedure was implemented based on Mathematical Morphological Analysis. The seminal work of Bandt-Pompe Permutation Entropy [15] also explores succinctly this idea as a basis to establish the time series ordinal patterns. In the article [16], the authors introduce a method for classification of rhythmic EEG events like Visual Occipital Alpha Waves and Motor Imagery Rolandic Central  $\mu$  Rhythms using the Histogram of Gradient Orientations of signal plots. Inspired in that work, we propose a novel application of the developed method to classify and describe transient events, particularly the P300 Event Related Potential. The proposed approach is based on the waveform analysis of the shape of the EEG signal. The signal is drawn on a bidimensional image plot, vector gradients of pixels around the plot are obtained, and with them, the histogram of their orientations is calculated. This histogram is a direct representation of the waveform of the signal. The method is built by mimicking what regularly electroencephalographers have been performing for almost a century as it is described in [17]: visually inspecting raw signal plots.

This paper reports a method to, (1) describe a procedure to capture the shape of a waveform of an ERP component, the P300, using histograms of gradient orientations extracted

R. Ramele, A.J.Villar and J.M.Santos are with the Department of Computer Engineering, Instituto Tecnológico de Buenos Aires (ITBA), Ciudad de Buenos Aires, Argentina e-mail: rramele@itba.edu.ar

Manuscript received April 19, 2005; revised August 26, 2015.

from images of signal plots, and (2) outline the way in which this procedure can be used to implement an P300-Based BCI Speller application. Its validity is verified by offline processing two datasets, one of data from ALS patients and another one from data of healthy subjects.

This article unfolds as follows: Section II-A is dedicated to explain the Feature Extraction method based on Histogram of Gradient Orientations of the Signal Plot: Section II-A1 shows the preprocessing pipeline, Section II-A2 describes the image generation of the signal plot, Section II-A3 presents the feature extraction procedure while Section II-A4 introduces the Speller Matrix Letter Identification procedure. In Section III, the experimental protocol is expounded. Section IV shows the results of applying the proposed technique. In the final Section V we expose our remarks, conclusions and future work.

## II. MATERIALS AND METHODS

The P300 [18], [19] is a positive deflection of the EEG signal which occurs around 300 ms after the onset of a rare and deviant stimulus that the subject is expected to attend. It is produced under the oddball paradigm [3] and it is consistent across different subjects. It has a lower amplitude ( $\pm 5\mu V$ ) compared to basal EEG activity, reaching a Signal to Noise Ratio (SNR) of around  $-15$  db estimated based on the amplitude of the P300 response signal divided by the standard deviation of the background EEG activity [20]. This signal can be used to implement a speller application by means of a Speller Matrix [18]. This matrix is composed of 6 rows and 6 columns of numbers and letters. The subject can focus on one character of the matrix. Figure 1 shows an example of the Speller Matrix used in the OpenVibe open source software [21], where the flashes of rows and columns provide the deviant stimulus required to elicit this physiological response. Each time a row or a column that contains the desired letter flashes, the corresponding synchronized EEG signal should also contain the P300 signature and by detecting it, the selected letter can be identified.



Fig. 1: Example of the  $6 \times 6$  Speller Matrix used in the study obtained from the OpenVibe software. Rows and columns flash in random permutations.

### A. Feature Extraction from Signal Plots

In this section, the signal preprocessing, the method for generating images from signal plots, the feature extraction procedure and the Speller Matrix identification are described. Figure 2 shows a scheme of the entire process.

1) *Preprocessing Pipeline*: The data obtained by the capturing device is digitalized and a multichannel EEG signal is constructed.

The 6 rows and 6 columns of the Speller Matrix are intensified providing the visual stimulus. The number of a row or column is a location. A sequence of twelve randomly permuted locations  $l$  conform an intensification sequence. The whole set of twelve intensifications is repeated  $k_a$  times.

- **Signal Enhancement**: This stage consists of the enhancement of the SNR of the P300 pattern above the level of basal EEG. The pipeline starts by applying a notch filter to the raw digital signal, a 4th degree 10 Hz lowpass Butterworth filter and finally a decimation with a Finite Impulse Response (FIR) filter of order 30 from the original sampling frequency down to 16 Hz [22].
- **Artifact Removal**: For every complete sequence of 12 intensifications of 6 rows and 6 columns, a basic artifact elimination procedure is implemented by removing the entire sequence when any signal deviates  $\pm 70\mu V$ .
- **Segmentation**: For each of the 12 intensifications of one intensification sequence, a segment  $S_i^l$  of a window of  $t_{max}$  seconds of the multichannel signal is extracted, starting from the stimulus onset, corresponding to each row/column intensification  $l$  and to the intensification sequence  $i$ . As intensifications are permuted in a random order, the segments are rearranged corresponding to row flickering, labeled 1-6, whereas those corresponding to column flickering are labeled 7-12. Two of these segments should contain the P300 ERP signature time-locked to the flashing stimulus, one for the row, and one for the column.
- **Signal Averaging**: The P300 ERP is deeply buried under basal EEG so the standard approach to identify it is by point-to-point averaging the time-locked stacked signal segments. Hence the values which are not related to, and not time-locked to the onset of the stimulus are canceled out [23].

This last step determines the operation of any P300 Speller. In order to obtain an improved signal in terms of its SNR, repetitions of the sequence of row/column intensification are necessary. And, at the same time, as long as more repetitions are needed, the ability to transfer information faster is diminished, so there is a trade-off that must be acutely determined.

The procedure to obtain the point-to-point averaged signal goes as follows:

- 1) Highlight randomly the rows and columns from the matrix. There is one row and one column that should match the letter selected by the subject.
- 2) Repeat step 1  $k_a$  times, obtaining the segments  $S_1^l(n, c), \dots, S_{k_a}^l(n, c)$ , with  $1 \leq l \leq 12$ , of the EEG signal where the variables  $1 \leq n \leq n_{max}$

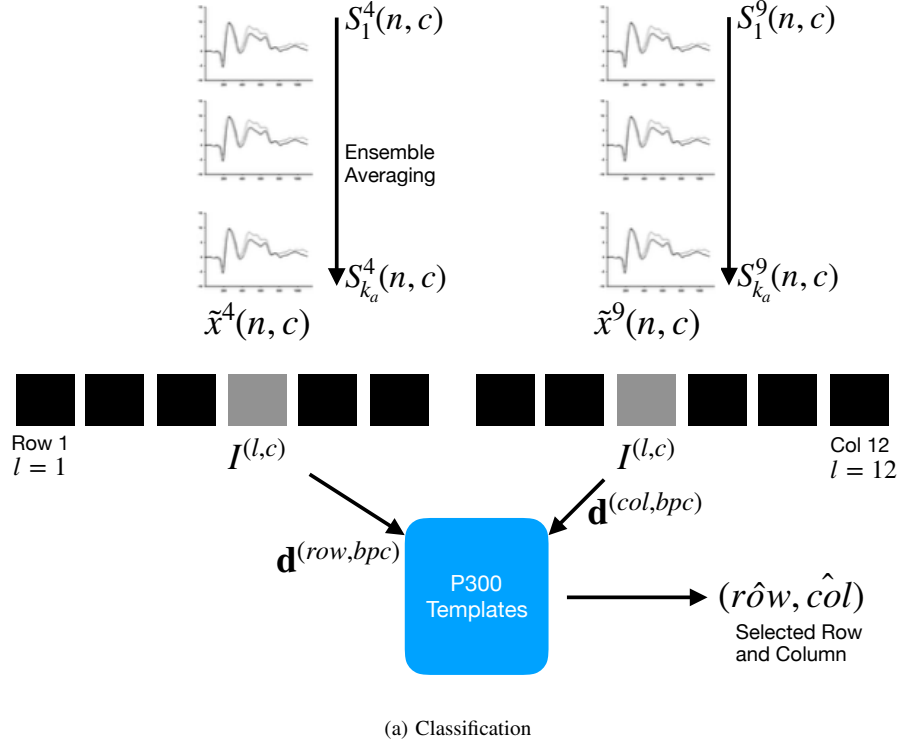


Fig. 2: For each column and row, an averaged, standardized and scaled signal  $\tilde{x}^l(n, c)$  is obtained from the segments  $S_i^l$  corresponding to the  $k_a$  intensification sequences with  $1 \leq i \leq k_a$  and location  $l$  varying between 1 and 12. From the averaged signal, the image  $I^{(l,c)}$  of the signal plot is generated and each descriptor is computed. By comparing each descriptor against the set of templates, the P300 ERP can be detected, and finally the desired letter from the matrix can be inferred.

and  $1 \leq c \leq C$  correspond to sample points and channel, respectively. The parameter  $C$  is the number of available EEG channels whereas  $n_{max} = F_s t_{max}$  is the segment length and  $F_s$  is the sampling frequency. The parameter  $k_a$  is the number of repetitions of intensifications and it is an input parameter of the algorithm.

3) Compute the Ensemble Average by

$$x^l(n, c) = \frac{1}{k_a} \sum_{i=1}^{k_a} S_i^l(n, c) \quad (1)$$

for  $1 \leq n \leq n_{max}$  and for the channels  $1 \leq c \leq C$ . This provide an averaged signal  $x^l(n, c)$  for the twelve locations  $1 \leq l \leq 12$ .

2) *Signal Plotting*: Averaged signal segments are standardized and scaled for  $1 \leq n \leq n_{max}$  and  $1 \leq c \leq C$  by

$$\tilde{x}^l(n, c) = \left\lceil \gamma \frac{(x^l(n, c) - \bar{x}^l(c))}{\hat{\sigma}^l(c)} \right\rceil \quad (2)$$

where  $\gamma > 0$  is an input parameter of the algorithm and it is related to the image scale. In addition,  $x^l(n, c)$  is the point-to-point averaged multichannel EEG signal for the sample point  $n$  and for channel  $c$ . Lastly,

$$\bar{x}^l(c) = \frac{1}{n_{max}} \sum_{n=1}^{n_{max}} x^l(n, c)$$

and

$$\hat{\sigma}^l(c) = \left( \frac{1}{n_{max} - 1} \sum_{n=1}^{n_{max}} (x^l(n, c) - \bar{x}^l(c))^2 \right)^{\frac{1}{2}}$$

are the mean and estimated standard deviation of  $x^l(n, c)$ ,  $1 \leq n \leq n_{max}$ , for each channel  $c$ .

Consequently, a binary image  $I^{(l,c)}$  is constructed according to

$$I^{(l,c)}(z_1, z_2) = \begin{cases} 255 & \text{if } z_1 = \gamma n \text{ and } z_2 = \tilde{x}^l(n, c) + z^l(c) \\ 0 & \text{otherwise} \end{cases} \quad (3)$$

with 255 being white and representing the signal's value location and 0 for black which is the background contrast, conforming a black-and-white plot of the signal. Pixel arguments  $(z_1, z_2) \in \mathbb{N} \times \mathbb{N}$  iterate over the width (based on the length of the signal segment) and height (based on the peak-to-peak amplitude) of the newly created image with  $1 \leq n \leq n_{max}$  and  $1 \leq c \leq C$ . The value  $z^l(c)$  is the image vertical position where the signal's zero value has to be situated in order to fit the entire signal within the image for each channel  $c$ :

$$z^l(c) = \left\lfloor \min_n \tilde{x}^l(n, c) \right\rfloor$$

where the minimization and maximization are carried out for  $n$  varying between  $1 \leq n \leq n_{max}$ , and  $\lfloor \cdot \rfloor$  denote the rounding to the smaller nearest integer of the number. This

value represents the length of the positive peak of the signal because the signal is inverted before the plot is constructed.

In order to complete the plot  $I^{(l,c)}$  from the pixels, the Bresenham [24], [16] algorithm is used to interpolate straight lines between each pair of consecutive pixels.

3) *Feature Extraction: Histogram of Gradient Orientations:* For each generated image  $I^{(l,c)}$ , a keypoint  $\mathbf{p}_k$  is placed on a pixel  $(x_{p_k}, y_{p_k})$  over the image plot and a window around the keypoint is considered. A local image patch of size  $X_p \times X_p$  pixels is constructed by dividing the window in 16 blocks of size  $3s$  each one, where  $s$  is the scale of the local patch and it is an input parameter of the algorithm. It is arranged in a  $4 \times 4$  grid and the pixel  $\mathbf{p}_k$  is the patch center, thus  $X_p = 12s$  pixels.

A local representation of the signal shape within the patch can be described by obtaining the gradient orientations on each of the 16 blocks  $B_{i,j}$  with  $0 \leq i, j \leq 3$  and creating a histogram of gradients. This technique is based on Lowe's SIFT [25] method, and it is biomimetically inspired in how the visual cortex detects shapes by analyzing orientations [26]. In order to calculate the histogram, the interval  $[0, 360]$  of possible angles is divided in 8 bins, each one of 45 degrees.

Hence, for each spatial bin  $0 \leq i, j \leq 3$ , corresponding to the indexes of each block  $B_{i,j}$ , the orientations are accumulated in a 3-dimensional histogram  $h$  through the following equation:

$$h(\theta, i, j) = 3s \sum_{\mathbf{p} \in I^{(l,c)}} w_{\text{ang}}(\angle J(\mathbf{p}) - \theta) w_{ij} \left( \frac{\|\mathbf{p} - \mathbf{p}_k\|}{3s} \right) |J(\mathbf{p})| \quad (4)$$

where  $\mathbf{p}$  is a pixel from the image  $I^{(l,c)}$ ,  $\theta$  is the angle bin with  $\theta$  belonging to  $\{0, 45, 90, 135, 180, 225, 270, 315\}$ ,  $|J(\mathbf{p})|$  is the norm of the gradient vector in the pixel  $\mathbf{p}$  and it is computed using finite differences and  $\angle J(\mathbf{p})$  is the angle of the gradient vector. The scalar  $w_{\text{ang}}(\cdot)$  and vector  $w_{ij}(\cdot)$  functions are linear interpolations used by [25] and [27] to provide a weighting contribution to eight adjacent bins. They are calculated as

$$w_{ij}(\mathbf{v}) = w(v_x - x_i)w(v_y - y_j) \quad (5)$$

with  $0 \leq i, j \leq 3$  and

$$w_{\text{ang}}(\alpha) = \sum_{r=-1}^1 w \left( \frac{8\alpha}{2\pi} + 8r \right) \quad (6)$$

where  $x_i$  and  $y_j$  are the spatial bin centers located in  $x_i, y_j \in \{-\frac{3}{2}, -\frac{1}{2}, \frac{1}{2}, \frac{3}{2}\}$ ,  $\mathbf{v} = (v_x, v_y)$  is a vector variable and  $\alpha$  a scalar variable. On the other hand,  $r$  is an integer that can vary freely between  $[-1, 1]$  which allows the argument  $\alpha$  to be unconstrained in terms of its values in radians. The interpolating function  $w(\cdot)$  is defined as  $w(z) = \max(0, |z| - 1)$ .

These binning functions conform a trilinear interpolation that has a combined effect of sharing the contribution of each oriented gradient between their eight adjacent bins in a tridimensional cube in the histogram space, and zero everywhere else.

Lastly, the fixed value of 3 is a magnification factor which corresponds to the number of pixels per each block when  $s = 1$ . As the patch has 16 blocks and 8 bin angles are considered, for each location  $l$  and channel  $c$  a feature called *descriptor*  $\mathbf{d}^{(l,c)}$  of 128 dimension is obtained.

Figure 3 shows an example of a patch and a scheme of the histogram computation. In (A) a plot of the signal and the patch centered around the keypoint is shown. In (B) the possible orientations on each patch are illustrated. Only the upper-left four blocks are visible. The first eight orientations of the first block, are labeled from 1 to 8 clockwise. The orientations of the second block  $B_{1,2}$  are labeled from 9 to 16. This labeling continues left-to-right, up-down until the eight orientations for all the sixteen blocks are assigned. They form the corresponding descriptor  $\mathbf{d}$  of 128 coordinates. Finally, in (C) an enlarged image plot is shown where the oriented gradient vector for each pixel can be seen.

4) *Speller Matrix letter Identification:*

a) *P300 ERP Extraction:* Segments corresponding to row flickering are labeled 1-6, whereas those corresponding to column flickering are labeled 7-12. The extraction process has the following steps:

- **Step A:** First highlight rows and columns from the matrix in a random permutation order and obtain the Ensemble Average as detailed in steps 1, 2 and 3 in Section II-A1.
- **Step B:** Plot the signals  $\tilde{x}^l(n, c)$ ,  $1 \leq n \leq n_{\text{max}}$ ,  $1 \leq c \leq C$ , according Section II-A2 in order to generate the images  $I^{(l,c)}$  for rows and columns  $1 \leq l \leq 12$ .
- **Step C:** Obtain the descriptors  $\mathbf{d}^{(l,c)}$  for rows and columns from  $I^{(l,c)}$  in accordance to the method described in Section II-A3.

b) *Calibration:* A trial, as defined by the BCI2000 platform [28], is every attempt to select just one letter from the speller. A set of trials is used for calibration and once the calibration is complete it can be used to identify new letters from new trials.

During the calibration phase, two descriptors  $\mathbf{d}^{(l,c)}$  are extracted for each available channel, corresponding to the locations  $l$  of a selection of one previously instructed letter from the set of calibration trials. These descriptors are the P300 templates, grouped together in a template set called  $T^c$ . The set is constructed using the steps described in Section II-A1 and the steps A, B and C of the P300 ERP extraction process.

Additionally, the best performing channel,  $bpc$  is identified based on the the channel where the best Character Recognition Rate is obtained.

c) *Letter identification:* In order to identify the selected letter, the template set  $T^{bpc}$  is used as a database. Thus, new descriptors are computed and they are compared against the descriptors belonging to the calibration template set  $T^{bpc}$ .

- **Step D:** Match to the calibration template  $T^{bpc}$  by computing

$$r\hat{ow} = \arg \min_{l \in \{1, \dots, 6\}} \sum_{q \in N_T(\mathbf{d}^{(l,bpc)})} \left\| q - \mathbf{d}^{(l,bpc)} \right\|^2 \quad (7)$$

and

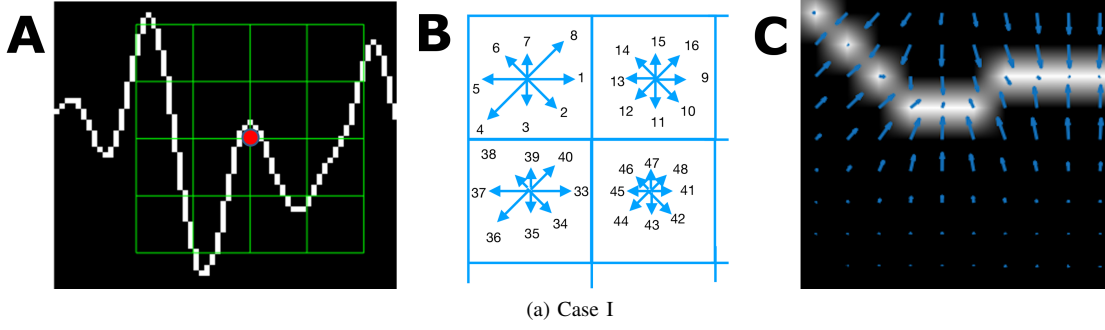


Fig. 3: (A) Example of a plot of the signal, a keypoint and the corresponding patch. (B) A scheme of the orientation's histogram computation. Only the upper-left four blocks are visible. The first eight orientations of the first block, are labeled from 1 to 8 clockwise. The orientation of the second block  $B_{1,2}$  is labeled from 9 to 16. This labeling continues left-to-right, up-down until the eight orientations for all the sixteen blocks are assigned. They form the corresponding descriptor of 128 coordinates. The length of each arrow represent the value of the histogram on each direction for each block. (C) Vector field of oriented gradients. Each pixel is assigned an orientation and magnitude calculated using finite differences.

$$\hat{col} = \arg \min_{l \in \{7, \dots, 12\}} \sum_{q \in N_T(\mathbf{d}^{(l, bpc)})} \|q - \mathbf{d}^{(l, bpc)}\|^2 \quad (8)$$

where  $N_T(\mathbf{d}^{(l, bpc)})$  is defined as  $N_T(\mathbf{d}^{(l, bpc)}) = \{\mathbf{d} \in T^{bpc} / \text{is the } k\text{-nearest neighbor of } \mathbf{d}^{(l, bpc)}\}$  for the best performing channel. This set is obtained by sorting all the elements in  $T^{bpc}$  based on distances between them and  $\mathbf{d}^{(l, bpc)}$ , choosing the  $k$  with smaller values, with  $k$  a parameter of the algorithm. This procedure is based on the k-NBNN algorithm [29].

By computing the aforementioned equations, the letter of the matrix can be determined from the intersection of the row  $row$  and column  $col$ . Figure 2 shows a scheme of this process.

### III. EXPERIMENTAL PROTOCOL

To verify the validity of the proposed framework and method, the public dataset 008-2014 [30] published on the BNCI-Horizon website [31] by IRCCS Fondazione Santa Lucia, is used. Additionally, an own dataset with the same experimental conditions is generated. Both of them are utilized to perform an offline BCI Simulation to decode the spelled words from the provided signals.

The algorithm is implemented using VLFeat [27] Computer Vision libraries on MATLAB V2014a (Mathworks Inc., Natick, MA, USA). Furthermore, for a sake of reproducibility, the code of the algorithm has been made available at: <https://bitbucket.org/itba/hist>.

In the following sections the characteristics of the datasets and parameters of the identification algorithm are described.

#### A. P300 ALS Public Dataset

The experimental protocol used to generate this dataset is explained in [30] but can be summarized as follows: 8 subjects with confirmed diagnoses but on different stages of ALS disease, were recruited and accepted to perform the experiments. The Visual P300 detection task designed for this experiment consisted of spelling 7 words of 5 letters each,

using the traditional P300 Speller Matrix [18]. The flashing of rows and columns provide the deviant stimulus required to elicit this physiological response. The first 3 words are used for calibration and the remaining 4 words, for testing with visual feedback. A trial is every attempt to select a letter from the speller. It is composed of signal segments corresponding to  $k_a = 10$  repetitions of flashes of 6 rows and  $k_a = 10$  repetitions of flashes of 6 columns of the matrix, yielding 120 repetitions. Flashing of a row or a column is performed for 0.125 s, following by a resting period (i.e. inter-stimulus interval) of the same length. After 120 repetitions an inter-trial pause is included before resuming with the following letter.

The recorded dataset was sampled at 256 Hz and it consisted of a scalp multichannel EEG signal for electrode channels Fz, Cz, Pz, Oz, P3, P4, PO7 and PO8, identified according to the 10-20 International System, for each one of the 8 subjects. The recording device was a research-oriented digital EEG device (g.Mobilab, g.Tec, Austria) and the data acquisition and stimuli delivery were handled by the BCI2000 open source software [28].

In order to assess and verify the identification of the P300 response, subjects are instructed to perform a copy-spelling task. They have to fix their attention to successive letters for copying a previously determined set of words, in contrast to a free-running operation of the speller where each user decides on its own what letter to choose.

#### B. P300 for healthy subjects

We replicate the same experiment on healthy subjects using a wireless digital EEG device (g.Nautilus, g.Tec, Austria). The experimental conditions are the same as those used for the previous dataset, as detailed in section III-A. The produced dataset is available in a public online repository [32].

Participants are recruited voluntarily and the experiment is conducted anonymously in accordance with the Declaration of Helsinki published by the World Health Organization. No monetary compensation is handed out and all participants agree and sign a written informed consent. This study is approved by the *Departamento de Investigación y Doctorado*,



*Instituto Tecnológico de Buenos Aires (ITBA)*. All healthy subjects have normal or corrected-to-normal vision and no history of neurological disorders. The experiment is performed with 8 subjects, 6 males, 2 females, 6 right-handed, 2 left-handed, average age 29.00 years, standard deviation 11.56 years, range 20-56 years.

EEG data is collected in a single recording session. Participants are seated in a comfortable chair, with their vision aligned to a computer screen located one meter in front of them. The handling and processing of the data and stimuli is conducted by the OpenVibe platform [21].

Gel-based active electrodes (g.LADYbird, g.Tec, Austria) are used on the same positions Fz, Cz, Pz, Oz, P3,P4, PO7 and PO8. Reference is set to the right ear lobe and ground is preset as the AFz position. Sampling frequency is slightly different, and is set to 250 Hz, which is the closest possible to the one used with the other dataset.

### C. Parameters

The patch size is  $X_P = 12s \times 12s$  pixels, where  $s$  is the scale of the local patch and it is an input parameter of the algorithm. The P300 event can have a span of 400 ms and its amplitude can reach  $10\mu V$  [33]. Hence it is necessary to utilize a signal segment of size  $t_{max} = 1$  second and a size patch  $X_P$  that could capture an entire transient event. With this purpose in consideration, the  $s$  value election is essential.

We propose the Equations 10 and 11 to compute the scale value in horizontal and vertical directions, respectively.

$$s_x = \frac{\gamma \lambda F_s}{12} \quad (9)$$

$$s_y = \frac{\gamma \Delta\mu V}{12} \quad (10)$$

where  $\lambda$  is the length in seconds covered by the patch,  $F_s$  is the sampling frequency of the EEG signal (downsampled to 16 Hz) and  $\Delta\mu V$  corresponds to the amplitude in microvolts that can be covered by the height of the patch. The geometric structure of the patch forces a squared configuration, then we discerned that by using  $s = s_x = s_y = 3$  and  $\gamma = 4$ , the local patch and the descriptor can identify events of  $9\mu V$  of amplitude, with a span of  $\lambda = 0.56$  seconds. This also determines that 1 pixel represents  $\frac{1}{\gamma} = \frac{1}{4}\mu V$  on the vertical direction and  $\frac{1}{F_s \gamma} = \frac{1}{64}$  seconds on the horizontal direction. The keypoints  $\mathbf{p}_k$  are located at  $(x_{p_k}, y_{p_k}) = (0.55F_s \gamma, z^l(c)) = (35, z^l(c))$  for the corresponding channel  $c$  and location  $l$  (see Equation 4). In this way the whole transient event is captured. Figure 4 shows a patch of a signal plot covering the complete amplitude (vertical direction) and the complete span of the signal event (horizontal direction).

Lastly, the number of channels  $C$  is equal to 8 for both datasets, and the number of intensification sequences  $k_a$  is fixed to 10. The parameter  $k$  used to construct the set  $N_T(\mathbf{d}^{(l,c)})$  is assigned to  $k = 7$ , which was found empirically to achieve better results. In addition, the norm used on Equations 8 and 9 is the cosine norm, and descriptors are normalized to  $[-1, 1]$ .

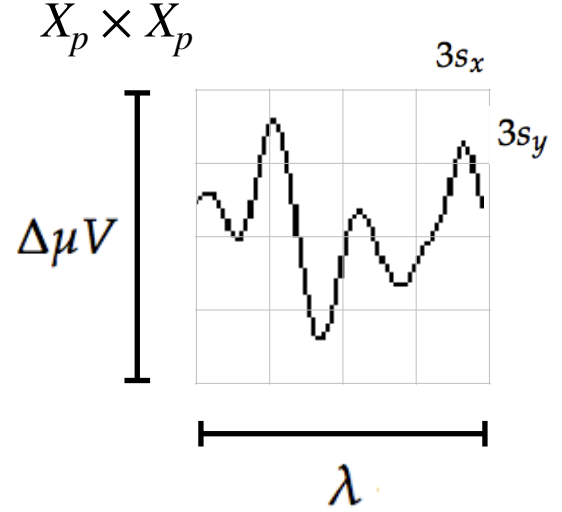


Fig. 4: The scale of local patch is selected in order to capture the whole transient event. The size of the patch is  $X_p \times X_p$  pixels. The vertical size consists of 4 blocks of size  $3s_y$  pixels which is high enough as to contain the signal  $\Delta\mu V$ , the peak-to-peak amplitude of the transient event. The horizontal size includes 4 blocks of  $3s_x$  and covers the entire duration in seconds of the transient signal event,  $\lambda$ .

## IV. RESULTS

Table I shows the results of applying the Histogram of Gradient Orientations (HIST) algorithm to the subjects of the public dataset of ALS patients. The percentage of correctly spelled letters is calculated while performing an offline BCI Simulation. From the seven words for each subject, the first three are used for calibration, and the remaining four are used for testing. The best performing channel  $bpc$  is informed as well. The target ratio is 1 : 36; hence theoretical chance level is 2.8%. It can be observed that the best performance of the letter identification method is reached in a dissimilar channel depending on the subject being studied.

TABLE I: Character recognition rates for the public dataset of ALS patients using the Histogram of Gradient (HIST) calculated from single-channel plots. Performance rates using single-channel signals with the SVM classifier are shown for comparison. The best performing channel  $bpc$  for each method is visualized

Participant	$bpc$	HIST	$bpc$	Single Channel SVM
1	Cz	35%	Cz	15%
2	Fz	85%	PO8	25%
3	Cz	25%	Fz	5%
4	PO8	55%	Oz	5%
5	PO7	40%	P3	25%
6	PO7	60%	PO8	20%
7	PO8	80%	Fz	30%
8	PO7	95%	PO7	85%

Table I and II show for comparison the obtained performance rates using single-channel signals with the Support Vec-

tor Machine (SVM) [34] classifier. This method is configured to use a linear kernel. The best performing channel, where the best letter identification rate was achieved, is also depicted.

TABLE II: Character recognition rates for the own dataset of healthy subjects using the Histogram of Gradient (HIST) calculated from single-channel plots. Performance rates using single-channel signals with the SVM classifier are shown for comparison. The best performing channel *bpc* for each method is visualized.

Participant	<i>bpc</i>	HIST	<i>bpc</i>	Single Channel SVM
1	Oz	40%	Cz	10%
2	PO7	30%	Cz	5%
3	P4	40%	P3	10%
4	P4	45%	P4	35%
5	P4	60%	P3	10%
6	Pz	50%	P4	25%
7	PO7	70%	P3	30%
8	P4	50%	PO7	10%

The Information Transfer Rate (ITR), or Bit Transfer Rate (BTR), in the case of reactive BCIs [3] depends on the amount of signal averaging required to transmit a valid and robust selection. Figure 5 shows the performance curves for varying intensification sequences for the subjects included in the dataset of ALS patients. It can be noticed that the percentage of correctly identified letters depends on the number of intensification sequences that are used to obtain the averaged signal. Moreover, when the number of intensification sequences tend to 1, which corresponds to single-intensification character recognition, the performance is reduced. As mentioned before, the SNR of the P300 obtained from only one segment of the intensification sequence is very low and the shape of its P300 component is not very well defined.

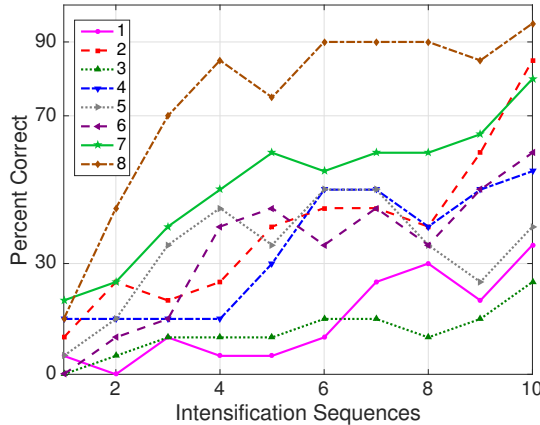


Fig. 5: Performance curves for the eight subjects included in the dataset of ALS patients. Three out of eight subjects achieved the necessary performance to implement a valid P300 speller.

In Table II the results obtained for 8 healthy subjects are shown. It can be observed that the performance is above chance level. It was verified that HIST method has an improved performance at letter identification than SVM that

process the signals on a channel by channel strategy (Wilcoxon signed-rank test,  $p = 0.004$  for both datasets).

Tables III and IV are presented in order to compare the performance of the HIST method versus a multichannel version of the Stepwise Linear Discriminant Analysis (SWLDA) and SVM classification algorithms for both datasets. The feature was formed by concatenating all the channels [22]. SWLDA is the methodology proposed by the ALS dataset's publisher. Since authors [30] did not report the Character Recognition Rate obtained for this dataset, we replicate their procedure and include the performance obtained with the SWLDA algorithm at letter identification. It was verified for the dataset of ALS patients that it has similar performance against other methods like SWLDA or SVM, which use a multichannel feature (Quade test with  $p = 0.55$ ) whereas for the dataset of healthy subjects significant differences were found (Quade test with  $p = 0.02$ ) where only the HIST method achieved a different performance than SVM (with multiple comparisons, significant difference of level 0.05).

TABLE III: Character recognition rates and the best performing channel *bpc* for the public dataset of ALS patients using the Histogram of Gradient (HIST) (repeated here for comparison purposes). Performance rates obtained by SWLDA and SVM classification algorithms with a multichannel concatenated feature.

Participant	<i>bpc</i> for HIST	HIST	Multichannel SWLDA	Multichannel SVM
1	Cz	35%	45%	40%
2	Fz	85%	30%	50%
3	Cz	25%	65%	55%
4	PO8	55%	40%	50%
5	PO7	40%	35%	45%
6	PO7	60%	35%	70%
7	PO8	80%	60%	35%
8	PO7	95%	90%	95%

TABLE IV: Character recognition rates and the best performing channel *bpc* for the own dataset of healthy subjects using the Histogram of Gradient (HIST) (repeated here for comparison purposes). Performance rates obtained by SWLDA and SVM classification algorithms with a multichannel concatenated feature.

Participant	<i>bpc</i> for HIST	HIST	Multichannel SWLDA	Multichannel SVM
1	Oz	40%	65%	40%
2	PO7	30%	15%	10%
3	P4	40%	50%	25%
4	P4	45%	40%	20%
5	P4	60%	30%	20%
6	Pz	50%	35%	30%
7	PO7	70%	25%	30%
8	P4	50%	35%	20%

The P300 ERP consists of two overlapping components: the P3a and P3b, the former with frontocentral distribution while the later stronger on centroparietal region [35]. Hence, the standard practice is to find the stronger response on the central channel Cz [30]. However, [22] show that the response may also arise in occipital regions. We found that by analyzing

only the waveforms, occipital channels PO8 and PO7 show higher performances for some subjects.

As subjects have varying *latencies* and *amplitudes* of their P300 components, they also have a varying stability of the *shape* of the generated ERP [36]. Figure 6 shows 10 sample P300 templates patches for patients 8 and 3 from the dataset of ALS patients. It can be discerned that in coincidence with the performance results, the P300 signature is more clear and consistent for subject 8 (A) while for subject 3 (B) the characteristic pattern is more difficult to perceive.

Additionally, the stability of the P300 component waveform has been extensively studied in patients with ALS [37], [38], [39], [40], [41] where it was found that these patients have a stable P300 component, which were also sustained across different sessions. In line with these results we do not find evidence of a difference in terms of the performance obtained by analyzing the waveforms (HIST) for the group of patients with ALS and the healthy group of volunteers (Mann-Whitney U Test,  $p = 0.46$ ). Particularly, the best performance is obtained for a subject from the ALS dataset for which, based on visual observation, the shape of the P300 component is consistently identified.

It is important to remark that when applied to binary images obtained from signal plots, the feature extraction method described in Section II-A3 generates sparse descriptors. Under this subspace we found that using the cosine metric yielded a significant performance improvement. On the other hand, the unary classification scheme based on the NBNN algorithm proved very beneficial for the P300 Speller Matrix. This is due to the fact that this approach solves the unbalance dataset problem which is inherent to the oddball paradigm [42].

## V. DISCUSSION

Among other applications of Brain Computer Interfaces, the goal of the discipline is to provide communication assistance to people affected by neuro-degenerative diseases, who are the most likely population to benefit from BCI systems and EEG processing and analysis.

In this work, a method to extract an objective metric from the waveform of the plots of EEG signals is presented. Its usage to implement a valid P300-Based BCI Speller application is expounded. Additionally, its validity is evaluated using a public dataset of ALS patients and an own dataset of healthy subjects.

It was verified that this method has an improved performance at letter identification than other methods that process the signals on a channel by channel strategy, and it even has a comparable performance against other methods like SWLDA or SVM, which uses a multichannel feature. Furthermore, this method has the advantage that shapes of waveforms can be analyzed in an objective way. We observed that the shape of the P300 component is more stable in occipital channels, where the performance for identifying letters is higher. We additionally verified that ALS P300 signatures are stable in comparison to those of healthy subjects.

We believe that the use of descriptors based on histogram of gradient orientation, presented in this work, can also be

utilized for deriving a shape metric in the space of the P300 signals which can complement other metrics based on time-domain as those defined by [40]. It is important to notice that the analysis of waveform shapes is usually performed in a qualitative approach based on visual inspection [37], and a complementary methodology which offer a quantitative metric will be beneficial to these routinely analysis of the waveform of ERPs.

### A. Conclusion

The goal of this work is to answer the question if a P300 component could be solely determined by inspecting automatically their waveforms. We conclude affirmatively, though two very important issues still remain:

First, the stability of the P300 in terms of its shape is crucial: the averaging procedure, montages, the signal to noise ratio and spatial filters all of them are non-physiological factors that affect the stability of the shape of the P300 ERP. We tested a preliminary approach to assess if the morphological shape of the P300 of the averaged signal can be stabilized by applying different alignments of the stacked segments (see Figure 2) and we verified that there is a better performance when a correct segment alignment is applied. We applied Dynamic Time Warping (DTW) [43] to automate the alignment procedure but we were unable to find a substantial improvement. Further work to study the stability of the shape of the P300 signature component needs to be addressed.

The second problem is the amplitude variation of the P300. We propose a solution by standardizing the signal, shown in Equation 2. It has the effect of normalizing the peak-to-peak amplitude, moderating its variation. It has also the advantage of reducing noise that was not reduced by the averaging procedure. It is important to remark that the averaged signal variance depends on the number of segments used to compute it [44]. The standardizing process converts the signal to unit signal variance which makes it independent of the number  $k_a$  of signals averaged. Although this is initially an advantageous approach, the standardizing process reduces the amplitude of any significant P300 complex diminishing its automatic interpretation capability.

In our opinion, the best benefit of the presented method is that a closer collaboration of the field of BCI with physicians can be fostered [45], since this procedure intent to imitate human visual observation. Automatic classification of patterns in EEG that are specifically identified by their shapes like K-Complex, Vertex Waves, Positive Occipital Sharp Transient [17] are a prospect future work to be considered. We are currently working in unpublished material analyzing K-Complex components that could eventually provide assistance to physicians to locate these EEG patterns, specially in long recording periods, frequent in sleep research [46]. Additionally, it can be used for artifact removal which is performed on many occasions by visually inspecting signals. This is due to the fact that the descriptors are a direct representation of the shape of signal waveforms. In line with these applications, it can be used to build a database [45] of quantitative representations of waveforms and improve atlases [17], which are currently based on qualitative descriptions of signal shapes.



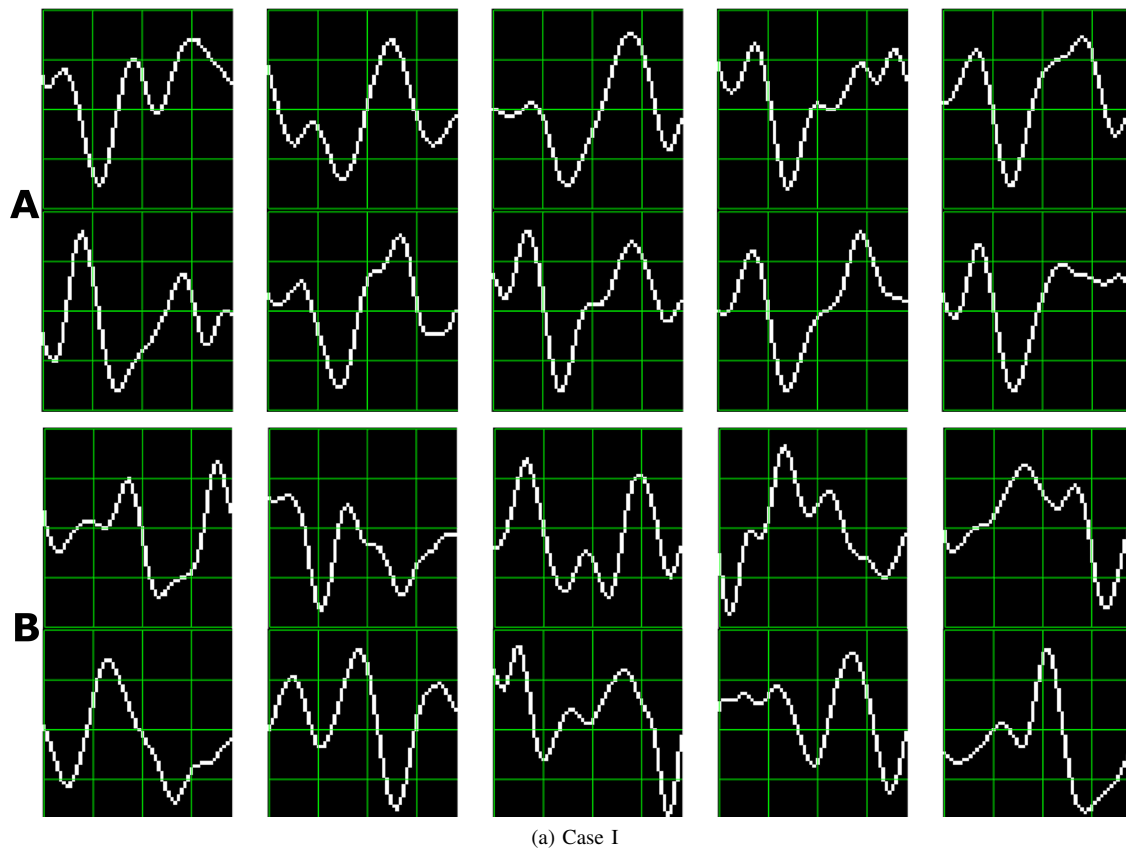


Fig. 6: Ten sample P300 template patches for subjects 8 (A) and 3 (B) of the ALS Dataset. Downward deflection is positive polarity.

## VI. ACKNOWLEDGMENTS

This project was supported by the ITBACyT-15 funding program issued by ITBA University from Buenos Aires, Argentina.

## CONFLICT OF INTEREST STATEMENT

The authors declare that the research was conducted in the absence of any commercial or financial relationships that could be construed as a potential conflict of interest.

## REFERENCES

- [1] D. L. Schomer and F. L. D. Silva, *Niedermeyer's Electroencephalography: Basic Principles, Clinical Applications, and Related Fields*. Walters Kluwer-Lippincott Williams & Wilkins, 2010.
- [2] M. De Vos and S. Debener, "Mobile EEG: Towards brain activity monitoring during natural action and cognition," *International Journal of Psychophysiology*, vol. 91, no. 1, pp. 1–2, 2014.
- [3] J. Wolpaw and W. E., *Brain-Computer Interfaces: Principles and Practice*. Oxford University Press, 2012. [Online]. Available: <http://books.google.com/books?hl=en&lr=&id=0dST2Lg4KVYC&pgis=1>
- [4] T. Carlson and J. del R. Millan, "Brain-controlled wheelchairs: A robotic architecture," *IEEE Robotics & Automation Magazine*, vol. 20, no. 1, pp. 65–73, mar 2013. [Online]. Available: <http://ieeexplore.ieee.org/document/6476692/>
- [5] C. Guger, S. Daban, E. Sellers, C. Holzner, G. Krausz, R. Carabalona, F. Gramatica, and G. Edlinger, "How many people are able to control a P300-based brain-computer interface (BCI)?" *Neuroscience Letters*, vol. 462, no. 1, pp. 94–98, 2009.
- [6] F. Lotte, J. Faller, C. Guger, Y. Renard, G. Pfurtscheller, A. Lécuyer, and R. Leeb, *Combining BCI with Virtual Reality: Towards New Applications and Improved BCI*. Springer Berlin Heidelberg, 2013, pp. 197 – 220.
- [7] F. Jure, L. Carrere, G. Gentiletti, and C. Tabernig, "BCI-FES system for neuro-rehabilitation of stroke patients," *Journal of Physics: Conference Series*, vol. 705, no. 1, pp. 1–8, 2016. [Online]. Available: <http://stacks.iop.org/1742-6596/705/i=1/a=012058?key=crossref.e4e42c8e6ea5d9ff10fe5b597ef6c490>
- [8] M. Clerc, L. Bougrain, and F. Lotte, *Brain-computer interfaces, Technology and applications 2(Cognitive Science)*. ISTE Ltd. and Wiley, 2016.
- [9] R. Riener and L. J. Seward, "Cyathlon 2016," *2014 IEEE International Conference on Systems, Man, and Cybernetics (SMC)*, pp. 2792–2794, oct 2014. [Online]. Available: <http://ieeexplore.ieee.org/lpdocs/epic03/wrapper.htm?arnumber=6974351>
- [10] D. Novak, R. Sigrist, N. J. Gerig, D. Wyss, R. Bauer, U. Gotz, and R. Riener, "Benchmarking brain-computer interfaces outside the laboratory: The cyathlon 2016," *Frontiers in Neuroscience*, vol. 11, p. 756, 2018. [Online]. Available: <https://www.frontiersin.org/article/10.3389/fnins.2017.00756>
- [11] C. Guger, B. Z. Allison, and M. A. Lebedev, "Introduction," in *Brain Computer Interface Research: A State of the Art Summary 6*. Springer, Cham, 2017, pp. 1–8. [Online]. Available: [http://link.springer.com/10.1007/978-3-319-64373-1\\_1](http://link.springer.com/10.1007/978-3-319-64373-1_1)
- [12] J. E. Huggins, R. E. Alcaide-Aguirre, and K. Hill, "Effects of text generation on P300 brain-computer interface performance," *Brain-Computer Interfaces*, vol. 3, no. 2, pp. 112–120, 2016. [Online]. Available: <http://www.tandfonline.com/doi/full/10.1080/2326263X.2016.1203629>
- [13] M. Alvarado-González, E. Garduño, E. Bribiesca, O. Yáñez-Suárez, and V. Medina-Bañuelos, "P300 Detection Based on EEG Shape Features," *Computational and Mathematical Methods in Medicine*, pp. 1–14, 2016. [Online]. Available: <http://www.hindawi.com/journals/cmmm/2016/2029791/>
- [14] T. Yamaguchi, M. Fujio, K. Inoue, and G. Pfurtscheller, "Design method of morphological structural function for pattern recognition of EEG signals during motor imagery and cognition," in *Fourth International Conference on Innovative Computing, Information and Control (ICICIC)*, 2009, pp. 1558–1561. [Online]. Available:

- <http://ieeexplore.ieee.org/document/5412503/>
- [15] S. Berger, G. Schneider, E. Kochs, and D. Jordan, "Permutation Entropy: Too Complex a Measure for EEG Time Series?" *Entropy* 2017, Vol. 19, Page 692, vol. 19, no. 12, p. 692, dec 2017. [Online]. Available: <http://www.mdpi.com/1099-4300/19/12/692>
  - [16] R. Ramele, A. J. Villar, and J. M. Santos, "BCI classification based on signal plots and SIFT descriptors," in *4th International Winter Conference on Brain-Computer Interface, BCI 2016*. Yongpyong: IEEE, feb 2016, pp. 1–4. [Online]. Available: <http://ieeexplore.ieee.org/document/7457454/>
  - [17] a. L. Hartman, *Atlas of EEG Patterns*. Lippincott Williams & Wilkins, 2005, vol. 65.
  - [18] L. A. Farwell and E. Donchin, "Talking off the top of your head: toward a mental prosthesis utilizing event-related brain potentials." *Electroencephalography and clinical neurophysiology*, vol. 70, no. 6, pp. 510–23, dec 1988. [Online]. Available: <http://www.ncbi.nlm.nih.gov/pubmed/2461285>
  - [19] K. H. Knuth, A. S. Shah, W. A. Truccolo, M. Ding, S. L. Bressler, and C. E. Schroeder, "Differentially variable component analysis: Identifying multiple evoked components using trial-to-trial variability," *Journal of Neurophysiology*, vol. 95, no. 5, pp. 3257–3276, 2006. [Online]. Available: <http://jn.physiology.org/content/95/5/3257>
  - [20] L. Hu, A. Mouraux, Y. Hu, and G. D. Iannetti, "A novel approach for enhancing the signal-to-noise ratio and detecting automatically event-related potentials (ERPs) in single trials," *NeuroImage*, vol. 50, no. 1, pp. 99–111, 2010. [Online]. Available: <http://dx.doi.org/10.1016/j.neuroimage.2009.12.010>
  - [21] Y. Renard, F. Lotte, G. Gibert, M. Congedo, E. Maby, V. Delannoy, O. Bertrand, and A. Lécuyer, "OpenViBE: An Open-Source Software Platform to Design, Test, and Use BrainComputer Interfaces in Real and Virtual Environments," *Presence: Teleoperators and Virtual Environments*, vol. 19, no. 1, pp. 35–53, feb 2010. [Online]. Available: <http://www.mitpressjournals.org/doi/10.1162/pres.19.1.35>
  - [22] D. J. Krusienski, E. W. Sellers, F. Cabestaing, S. Bayoudh, D. J. McFarland, T. M. Vaughan, and J. R. Wolpaw, "A comparison of classification techniques for the P300 Speller," *Journal of Neural Engineering*, vol. 3, no. 4, pp. 299–305, dec 2006. [Online]. Available: <http://www.ncbi.nlm.nih.gov/pubmed/17124334> <http://stacks.iop.org/1741-2552/3/i=4/a=007?key=crossref.0d0b93e9c0efb39f5c99794dfc099674>
  - [23] N. Liang and L. Bougrain, "Averaging techniques for single-trial analysis of oddball event-related potentials," *4th International Brain-Computer*, pp. 1–6, 2008. [Online]. Available: <http://hal.archives-ouvertes.fr/inria-00337070/>
  - [24] J. E. Bresenham, "Algorithm for computer control of a digital plotter," *IBM Systems Journal*, vol. 4, no. 1, pp. 25–30, 1965.
  - [25] G. Lowe, "SIFT - The Scale Invariant Feature Transform," *International Journal*, vol. 2, pp. 91–110, 2004.
  - [26] S. Edelman, N. Intrator, and T. Poggio, "Complex cells and object recognition," 1997. [Online]. Available: <http://cogprints.org/561/>
  - [27] A. Vedaldi and B. Fulkerson, "VLFeat - An open and portable library of computer vision algorithms," *Design*, vol. 3, no. 1, pp. 1–4, 2010. [Online]. Available: <http://vision.ucla.edu/~brian/papers/vedaldi10vlfeat.pdf>
  - [28] G. Schalk, D. J. McFarland, T. Hinterberger, N. Birbaumer, and J. R. Wolpaw, "BCI2000: a general-purpose brain-computer interface (BCI) system." *IEEE transactions on bio-medical engineering*, vol. 51, no. 6, pp. 1034–43, jun 2004. [Online]. Available: <http://www.ncbi.nlm.nih.gov/pubmed/15188875>
  - [29] O. Boiman, E. Shechtman, and M. Irani, "In defense of nearest-neighbor based image classification," *26th IEEE Conference on Computer Vision and Pattern Recognition, CVPR*, 2008.
  - [30] A. Riccio, L. Simone, F. Schettini, A. Pizzimenti, M. Inghilleri, M. O. Belardinelli, D. Mattia, and F. Cincotti, "Attention and P300-based BCI performance in people with amyotrophic lateral sclerosis," *Frontiers in Human Neuroscience*, vol. 7, no. November, p. 732, 2013. [Online]. Available: <http://www.pubmedcentral.nih.gov/articlerender.fcgi?artid=3825256&tool=pmcentrez&rendertype=abstract>
  - [31] C. Brunner, B. Blankertz, F. Cincotti, A. Kübler, D. Mattia, F. Miralles, A. Nijholt, and B. Otal, "BNCI Horizon 2020 Towards a Roadmap for Brain / Neural Computer Interaction," *Lecture Notes in Computer Science*, vol. 8513, no. 1, pp. 475–486, 2014.
  - [32] R. Ramele, A. J. Villar, and J. M. Santos, "P300-dataset rrid scr\_015977," <https://www.kaggle.com/rramele/p300samplingdataset>, 2017.
  - [33] R. P. N. Rao, *Brain-Computer Interfacing: An Introduction*. New York, NY, USA: Cambridge University Press, 2013.
  - [34] B. Scholkopf and A. J. Smola, *Learning with kernels: support vector machines, regularization, optimization, and beyond*. MIT press, 2001.
  - [35] J. Polich, "Updating P300: An integrative theory of P3a and P3b," *Clinical Neurophysiology*, vol. 118, no. 10, pp. 2128–2148, oct 2007.
  - [36] C. S. Nam, Y. Li, and S. Johnson, "Evaluation of P300-based brain-computer interface in real-world contexts," *International Journal of Human-Computer Interaction*, vol. 26, no. 6, pp. 621–637, may 2010. [Online]. Available: <http://www.tandfonline.com/doi/abs/10.1080/10447311003781326>
  - [37] E. W. Sellers, A. Kübler, and E. Donchin, "Brain-computer interface research at the University of South Florida cognitive psychophysiology laboratory: The P300 speller," *IEEE Transactions on Neural Systems and Rehabilitation Engineering*, vol. 14, no. 2, pp. 221–224, 2006.
  - [38] T. Madarame, H. Tanaka, T. Inoue, M. Kamata, and M. Shino, "The development of a brain computer interface device for amyotrophic lateral sclerosis patients," in *Conference Proceedings - IEEE International Conference on Systems, Man and Cybernetics*. IEEE, oct 2008, pp. 2401–2406. [Online]. Available: <http://ieeexplore.ieee.org/document/4811654/>
  - [39] F. Nijboer and U. Broermann, "Brain Computer Interfaces for Communication and Control in Locked-in Patients," in *Graimann B., Pfurtscheller G., Allison B. (eds) Brain-Computer Interfaces. The Frontiers Collection*. Springer Berlin Heidelberg, 2009, pp. 185–201. [Online]. Available: [http://link.springer.com/10.1007/978-3-642-02091-9\\_11](http://link.springer.com/10.1007/978-3-642-02091-9_11)
  - [40] J. N. Mak, D. J. McFarland, T. M. Vaughan, L. M. McCane, P. Z. Tsui, D. J. Zeitlin, E. W. Sellers, and J. R. Wolpaw, "EEG correlates of P300-based brain-computer interface (BCI) performance in people with amyotrophic lateral sclerosis," *Journal of Neural Engineering*, vol. 9, no. 2, 2012.
  - [41] L. M. McCane, S. M. Heckman, D. J. McFarland, G. Townsend, J. N. Mak, E. W. Sellers, D. Zeitlin, L. M. Tenteromano, J. R. Wolpaw, and T. M. Vaughan, "P300-based brain-computer interface (BCI) event-related potentials (ERPs): People with amyotrophic lateral sclerosis (ALS) vs. age-matched controls," *Clinical Neurophysiology*, vol. 126, no. 11, pp. 2124–2131, nov 2015. [Online]. Available: <http://www.ncbi.nlm.nih.gov/pubmed/25703940> <http://www.pubmedcentral.nih.gov/articlerender.fcgi?artid=PMC4529383>
  - [42] R. Tibon and D. A. Levy, "Striking a balance: analyzing unbalanced event-related potential data." *Frontiers in Neurophysiology*, vol. 6, p. 555, 2015. [Online]. Available: <http://www.ncbi.nlm.nih.gov/pubmed/25983716> <http://www.pubmedcentral.nih.gov/articlerender.fcgi?artid=PMC4416363>
  - [43] S. Casarotto, A. Bianchi, S. Cerutti, and G. Chiarenza, "Dynamic time warping in the analysis of event-related potentials," *IEEE Engineering in Medicine and Biology Magazine*, vol. 24, no. 1, pp. 68–77, 2005. [Online]. Available: <http://ieeexplore.ieee.org/document/1384103/>
  - [44] W. Van Drongeelen, *Signal processing for neuroscientists: an introduction to the analysis of physiological signals*. Academic press, 2006.
  - [45] R. Chavarriaga, M. Fried-Oken, S. Kleih, F. Lotte, and R. Scherer, "Heading for new shores! Overcoming pitfalls in BCI design," *Brain-Computer Interfaces*, vol. 4, no. 1-2, pp. 60–73, apr 2017. [Online]. Available: <https://www.tandfonline.com/doi/full/10.1080/2326263X.2016.1263916>
  - [46] C. M. Michel and M. M. Murray, "Towards the utilization of EEG as a brain imaging tool," *NeuroImage*, vol. 61, no. 2, pp. 371–385, jun 2012. [Online]. Available: <https://www.sciencedirect.com/science/article/pii/S1053811911014418>

Michael Shell Biography text here.



John Doe Biography text here.

**Jane Doe** Biography text here.